Nucleation-controlled vacancy formation in light-emitting wide-band-gap oxide nanocrystals in glass

N. V. Golubev,[a] E. S. Ignat'eva,[a] V. N. Sigaev,[a] L. De Trizio,[b] A. Azarbod,[cd] A. Paleari[ad]* and R. Lorenzi[d]

Light emission of nanocrystals (NCs) can depend not only on NC size but also – and even more importantly in wide-band-gap NCs – on the occurrence of optically active sites, such as donor-acceptor pairs (DAPs). Here, we demonstrate that controlling the thermo-chemical conditions of NC nucleation when NCs are forming in a solid host – an approach often used for driving NC size dispersion – can be an innovative strategy for tailoring DAP population. Our data show that light emission from DAP recombination and decay in defect sites can be controlled in γ-Ga_2O_3 NCs in alkali-germanosilicate glass – a prototypal oxide-in-oxide nanostructured system – by oxygen and gallium vacancy formation during nucleation. Time-resolved UV-excited photoluminescence, combined with differential scanning calorimetry, X-ray diffraction, and transmission electron microscopy, reveal how nucleation pretreatment determines, besides NC size and concentration, also DAP number via promotion of acceptor formation or their passivation during interaction with the host. The results envisage the possibility of nucleation-based design of light-emitting NCs in a wide range of oxide systems.

Introduction

Since the first work on quantum dots in glass, about 30 years ago,[1] the study of nanocrystal (NC) nucleation process has received great attention, initially for finely tuning NC size,[2] then for tailoring NC shape through smart solution-based routes.[3,4] Nevertheless, very recently, controlling NC structure and stoichiometry has become even more important than NC size, especially for incorporating dopant species or intrinsic defects – noticeably donor and acceptor sites – which can greatly determine the NC optical response.[5,6] In this regards, nucleation has been recently demonstrated to act as a powerful driving force for the incorporation of functional species, at least in prototypal Cd-based compounds.[7,8] Oxide-in-oxide NCs in inorganic matrices are instead more difficult to be controlled. Nevertheless, promising results have been obtained for SnO_2 and Ga_2O_3 NCs in silicate and germanate glasses, achieving glass-based easy-to-process bulk materials with efficient NC light emission and good optical transmittance of the resulting nanostructured system.[9-16] Nucleation mechanisms have been investigated in some of these oxides,[9-12] checking also the effects of dopant species,[13,14] in view of several possible applications, such as broadband light-emitters in the visible and IR region,[11,12,14,15] UV light-emitting-devices,[17,18] and solar-blind UV-to-visible optical converters.[19] However, no detailed study has yet been attempted to investigate nucleation effects on NC defectiveness, including donor and acceptor pairs (DAPs), despite they strongly determine the light emission yield, sometimes with unusual size-dependent features.[19-21]

Here, by means of time resolved photoluminescence (PL) spectroscopy as a sensitive probe of DAP recombination, aided by differential scanning calorimetry (DSC), X-ray diffraction (XRD), and transmission electron microscopy (TEM), we present the analysis of a system composed by Ga-oxide NCs in glass, as a prototypal wide-band-gap oxide-in-oxide system with good tendency to phase separation.[10,22] Our study gives a basis for understanding nucleation effects on DAP- and defect-dependent NC PL. The time-resolved analysis, from ns to μs domain, reveals the fine details of DAP decay, including not only acceptor-to-donor ratio-dependent hyperbolic decay, but also fast contributions from competitive decay channels never revealed up to now in glass-embedded Ga_2O_3 NCs. Importantly, the investigation of the kinetic features as a function of nucleation pre-treatments shows for the first time that Ga-oxide optical functions can be controlled - beyond any size dependent confinement effect - by controlling nanocrystal interactions with the surrounding host. As a result, our work suggests that DAP statistic and recombination in Ga_2O_3 can be designed in nanostructured glass through nucleation pre-treatment. Such an approach opens the way to new strategies of nucleation-based light emission design.

Experimental procedure

Glass with nominal composition 7.5Li_2O-2.5Na_2O-20Ga_2O_3-45GeO_2-25SiO_2 (mol%) was prepared by melt-quenching method. Raw materials were Li_2CO_3 (chemically pure), Na_2CO_3 (chemically pure), Ga_2O_3 (chemically pure), GeO_2 (special purity grade), SiO_2 (special purity grade). Starting materials were weighed using an analytical balance with an accuracy of 0.001 g. Reagents were thoroughly mixed in a beaker for 15-20 min. Glasses were prepared in an uncovered platinum crucible (~45 ml) in an electrically heated furnace at 1480 °C for 40 min. The melt was poured onto a stainless steel plate and quenched by pressing with another stainless steel plate obtaining samples about 2 mm thick. Energy-dispersive X-ray fluorescence microanalysis (Bruker, Artax 200) was carried out on as-quenched glass, obtaining evidence of uniform dispersion of the main elements (Ga, Ge, Si), consistently with analogous results collected by scanning electron microscopy equipped with a microprobe (Edax, Genesis 4000 XMS) on similar glass prepared by identical route for the production of optical fibre prototypes.[23] The as-quenched glass was cut with a low-speed diamond saw or grinding disc using water as a coolant. Samples were then polished for optical measurements or ground for XRD or TEM analysis. Part of as-quenched samples underwent nucleation pretreatment of 18 h in a muffle in the range 560-594 °C (accuracy ±2 K), placing the samples into the furnace at the treatment temperature and removing them from the hot furnace. Part of these samples was then treated for 30 min at the exothermic peak temperature, as determined by DSC measurements. In DSC measurements, a Netzsch DSC 449F3 thermoanalyzer was used, with a platinum pan with cover, 10 K

min^{-1} of heating rate of in Ar, using bulk samples of 10-15 mg. DSC peak temperature reproducibility is ±2 K. XRD patterns of powdered samples were recorded by means of a Bruker D2 Phaser diffractometer employing nickel-filtered CuKα radiation. FWHM of XRD reflections were identified by means of numerical subtraction of background and amorphous halo from the whole XRD pattern, and fitting nanophase reflections, by using the software Diffrac.Eva by Bruker. A Tecnai G2 F20 transmission electron microscope, equipped with a Schottky gun operated at 200 kV acceleration voltage, was used to acquire both high angle annular dark field (HAADF)-scanning TEM (STEM) images and high-resolution TEM images of the samples. Optical absorption spectra were collected by a Varian Cary50 spectrophotometer. Steady state PL, time-resolved PL spectra (5 nm of bandwidth), and PL decay (20 nm of bandwidth at 450 nm) were collected by means of an Edinburgh FLS980 fluorescence spectrometer with pulsed LED source at 250 nm (pulse duration 600 ps, repetition rate 500 ns or 50 μs). The uncertainty of relative PL intensity from excitation and light collection reproducibility is less than 10%.

Results and discussion

In Fig. 1a we report DSC curves of multi-component glass samples with composition $7.5Li_2O$-$2.5Na_2O$-$20Ga_2O_3$-$45GeO_2$-$25SiO_2$ (mol%) after nucleation pre-treatment for 18 h at different temperature T_n in the range 560-594 °C, compared with as-quenched untreated glass. The curves register an exothermic peak of crystallization at temperature T_c ranging between 648 and 667 °C, about 100 °C above the glass transition temperature T_g evidenced by a smooth step just above 550 °C. The temperature range of these two processes determines much of the system propensity to glass nanostructuring, since it determines glass stability, component diffusivity, and controllability of the crystallization process.[24] Between T_g and T_c, the present system gives rise to nucleation of a nanophase through formation of crystal nuclei from the progressive segregation of Ga-oxide-rich nano-droplets arising from native nano-heterogeneities, as indicated by small angle neutron scattering experiments.[10]

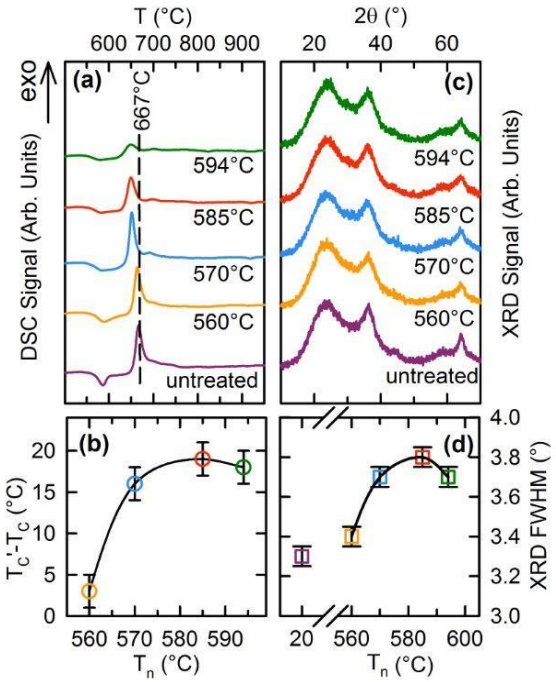

Figure 1. (a) DSC curves (vertically shifted for clarity) of glass with composition $7.5Li_2O$-$2.5Na_2O$-$20Ga_2O_3$-$45GeO_2$-$25SiO_2$ before (untreated) and after nucleation pre-treatment at the indicated temperatures for 18 h. (b) Shift of the exothermic DSC peak maximum temperature T_c in pretreated samples (with respect to T'_c of untreated sample) *vs.* nucleation pretreatment temperature T_n. (c) XRD patterns of the same samples (vertical order as in (a)) after subsequent treatment for 30 min at the exothermic peak temperature. (d) FWHM of γ-Ga_2O_3 XRD reflection at 36.3° *vs.* nucleation pretreatment temperature T_n. Curves in (b) and (d) are guides for the eyes.

This process shows some similarities to typical mixed oxides in the immiscibility region.[25] As a result, in the present system, pre-treatments at different temperature between T_g and T_c are expected to determine largely different conditions of crystalline nanostructuring, driven by different nucleation kinetics and resulting number of NC nuclei. In fact, the data show a non-monotonic shift of the exothermic peak temperature T_c as a result of pre-treatment (Fig. 1b), with a lowering from 667 °C (in untreated glass) to less than 650 °C in pretreated glass. Such a T_c lowering reflects the influence of pre-treatments on the number of nucleating sites, since the larger the number density of crystallization nuclei, the lower the crystallization temperature.[26] Theoretical and experimental studies on glass devitrification indeed established that nucleation rate and nuclei density number are maximized when the temperature shift T'_c-T_c between exothermic peak temperature in pre-treated (T_c) and untreated material (T'_c) is maximized.[27,28] Figure 1b suggests that the nucleation rate significantly changes in the investigated T_n range, with expected effects on the mean NC size. In Fig. 1c, we report XRD patterns of the same set of samples after treatment at T_c for 30 min. The data confirm the occurrence of pre-treatment effects on the full width at half maximum (FWHM) of the observed reflections, *i.e.* on the

mean NC size. Fitting the main XRD reflection of γ-Ga_2O_3 at 36.3°, we register FWHM modifications that resemble the T_n dependence of the exothermic DSC peak temperature (Figs. 1b, d). Quantitative comparison of the remaining glass fraction (estimated from the amorphous XRD halo) in treated samples gives evidence of approximately equal amount of crystalline γ-Ga_2O_3 nanophase in all the samples after the second treatment at T_c for 30 min, independently of T_n. Since the crystalline volume fraction $f_c=V_{NC}N_{NC}/V$ (where V_{NC} is the mean NC volume, N_{NC} the total NC number, and V is the total volume) does not depend on pre-treatment, the nucleation-dependent NC size also determines, as a result, NC density number N_{NC}/V. DSC and XRD analyses are qualitatively confirmed by TEM measurements (see Figs. 2a-d) and the related analysis of size distribution (Fig. 2e-h), at least within the experimental uncertainty. High resolution images show clear features ascribable to γ-Ga_2O_3 (Fig. 2d). However, consistently with the quite broad XRD patterns in Fig. 1c, the crystalline features in TEM images are quite reduced, suggesting a strong propensity to structural disorder. In this regards, the present glass-embedded system appears similar to recently investigated colloidal systems of disordered γ-Ga_2O_3 from particular synthesis routes.[29] The average size ranges from ~6 nm – in samples pretreated at low nucleation rates – to ~4 nm for faster nucleation rates. Interestingly, we also observe bimodal distribution of NC size (Fig. 2f,g), probably caused by coalescence mechanisms. It is to be remarked that a quantitative estimation of the mean nanocrystal size from XRD FWHM (for a direct comparison with TEM analysis) requires additional information on possible strain effects and size distribution. We have performed numerical simulations of the expected convolution of size distribution effects on the XRD FWHM (using TEM data as trial values for mean size and size distribution).

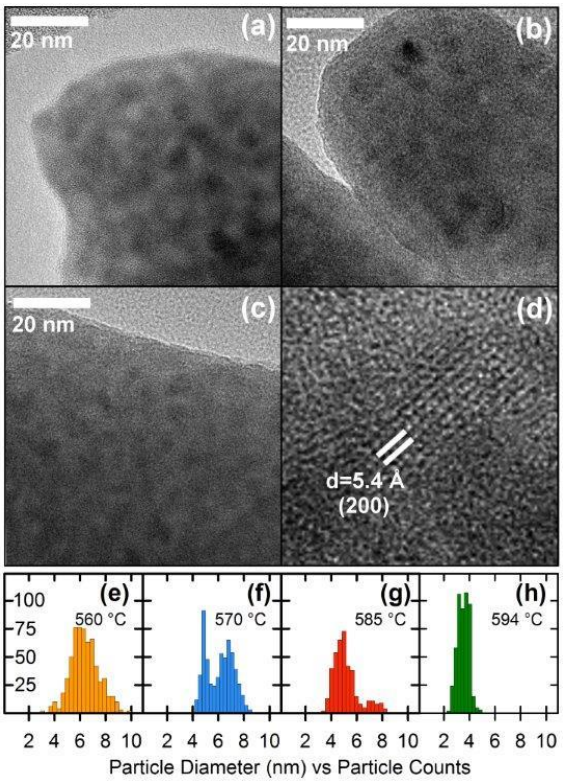

Figure 2. TEM images of nanocrystallized 7.5Li_2O-2.5Na_2O-20Ga_2O_3-45GeO_2-25SiO_2 samples treated 30 min at T_c after nucleation pre-treatment for 18 h at (a) 560 °C, 570 °C, and (c) 594 °C. (d) High resolution image of a NC with indication of crystal planes. From (e) to (h), histograms of NC size statistics from the analysis of several TEM images of samples treated at T_c after nucleation pre-treatment for 18 h at 560, 570, 585, and 594 °C, respectively.

The results suggest negligible effects compared with the effects of mean size change. It is instead likely that strains really influence the observed FWHM. However, the related effects are expected not to influence significantly the qualitative dependence of FWHM on nucleation pretreatment in Fig. 1d, since composition, nanostructuring, and host matrix properties are quite similar or even equal within the sample set. Interestingly, looking at Fig. 2e and 2f, the values of average nanocrystal size in samples pretreated at 560 and 570 °C - after second treatment at T_c - appear not so different as instead suggested by the quite distinct XRD FWHM values in Fig. 1d. Such a discrepancy – actually falling just outside the experimental uncertainty – is expected. In fact, the higher T_n, the lower is T_c (see Fig. 1a,b) and, in turn, the smaller is the coherent scattering (which is influenced by the crystallization temperature during the second treatment). By contrast, T_c of samples pretreated at 585 and 594 °C is almost equal (648 and 649 °C) and the second treatment of crystallization brings to comparable crystal domains. Anyway, both XRD and TEM analysis show a clear dependence on the nucleation rate during nucleation pretreatment.

Also the light emission properties of the material show to depend on the nucleation pre-treatment (Fig. 3). The luminescence spectrum excited at 5 eV – *i.e.* at energy higher than the optical absorption edge we observe at about 4.5 eV – consists of a broad band centered at 2.7-3.0 eV, 0.8-0.9 eV of FWHM. These features are typical of Ga oxide systems,[30] either bulk or nanostructured,[21,30] simple oxide or embedded in glass.[19,21] Such a PL band arises from radiative recombination of intrinsic band-

to-band excitations of Ga oxide at DAPs consisting of an oxygen vacancy, acting as a donor, and a complex of oxygen and gallium vacancies behaving as acceptors.[30] Interestingly, looking at the data in Fig. 3a, we notice that PL is observed even in only-pretreated material.

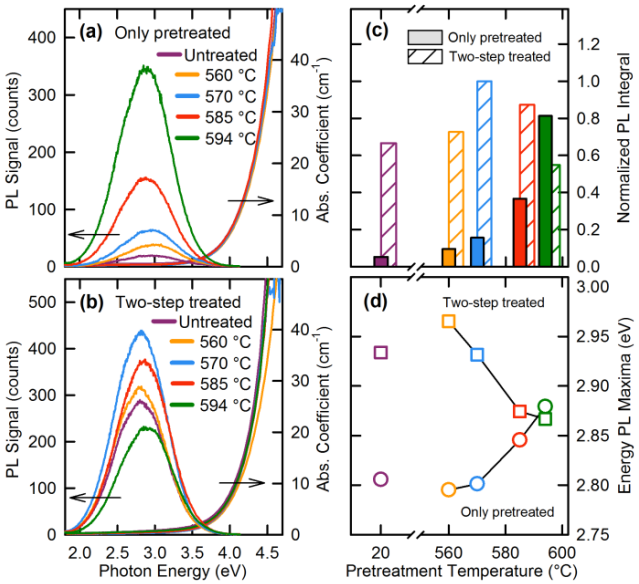

Figure 3. Steady-state 5 eV-excited PL spectra (left axis) and optical absorption (right axis) of $7.5Li_2O$-$2.5Na_2O$-$20Ga_2O_3$-$45GeO_2$-$25SiO_2$ before (a) and after (b) treatment of nanocrystallization at the exothermic peak extremum temperature T_c for 30 min, either in samples pretreated for 18 h at 560 °C, 570 °C, 585 °C, 594 °C, or not pretreated. (c) Dependence of PL intensity (from integration of spectra in (a) and (b)) on nucleation pretreatment temperature. (d) Dependence of PL band maximum (from spectra in (a) and (b)) on nucleation pretreatment temperature. Lines in (d) are guides for the eyes.

Furthermore, PL intensity is clearly influenced by T_n. Therefore, the crystallization nuclei formed in only-pretreated material turn out to be light emitting nano-systems with a PL spectrum that substantially resembles the spectral features of Ga-oxide. In only-pretreated samples, the intensity enhancement at increasing T_n (Fig. 3c) gives indication of DAP number increase, partially influenced by the change of number density of Ga-oxide nuclei. Importantly, as regards two-step treated samples, the T_n-dependence of PL intensity is non-monotonic (Figs. 3b and c), with a behavior similar to the effect of T_n on DSC, XRD and TEM data of Fig. 1b,d and Fig. 2. This fact suggests that NC number density $\rho(T_n)$ and NC size d probably play a key role in determining the PL intensity. On the one hand, $1/T_c$ is proportional to ρ,[26] and $[1/T_c–1/T'_c]$ is nearly proportional to $[T'_c–T_c]$ in the investigated T_n range. Therefore, the data of Fig. 1b should approximately reflect the deviation $\Delta\rho(T_n)$ of NC density with respect to material treated at T_c without nucleation pretreatment. On the other hand, the FWHM of XRD reflections in Fig. 1d is proportional to $1/d$ through the Scherrer's relation. Interestingly, the total cross section σ of NC optical excitation is indeed expected to depend on NC size just as $1/d$, at least if we suppose that σ depends on the product between the simple geometrical cross section of the single NC (proportional to d^2) and ρ, which in turn varies as d^{-3}. Taking into account that the crystalline fraction ξ after treatment at T_c is fixed by composition and does not vary by changing T_n, the qualitative agreement between data in Figs. 1b,d and in Fig. 3c points out the role of glass nanostructuring in the light emission photo-excitation process. However, the deviations from a quantitative agreement highlight the occurrence of a multiplicity of effects beyond the NC density.

A deeper analysis, based on time-resolved spectroscopic data (Fig. 4), indeed shows a more complex situation, in which different radiative decay mechanisms, from more than a single light emitting species, take part in the light emission process.Evidences of different spectral components underlying the broad PL band are indeed detected even in the steady-state PL measurements in Fig. 3d, in which spectral position of the PL band maximum shows energy shift apparently correlated with the intensity and accompanied by band shape changes. These features suggest the occurrence of different overlapping spectral components, whose relative intensity is influenced by the nucleation process (specifically by T_n), with spectral shape modifications and shift of the band maximum. Time-resolved PL spectra, both in the μs domain (Fig. 4a) and in the ns region (Fig. 4b), show analogous spectral shifts towards low energy during the decay process. Such red shifts concern two time intervals, after 15-25 ns from the pulse and in the range 10^{-1}-10^{0} μs. This result supports the occurrence of distinct light emission mechanisms responsible for PL contributions centered in slightly different spectral regions, with fast components at higher spectral energy, in the near UV, with respect to the slow component ascribed to DAP recombination, which is responsible for the main component in the blue region.

The occurrence of distinct light emission mechanisms is confirmed by PL decay kinetics.

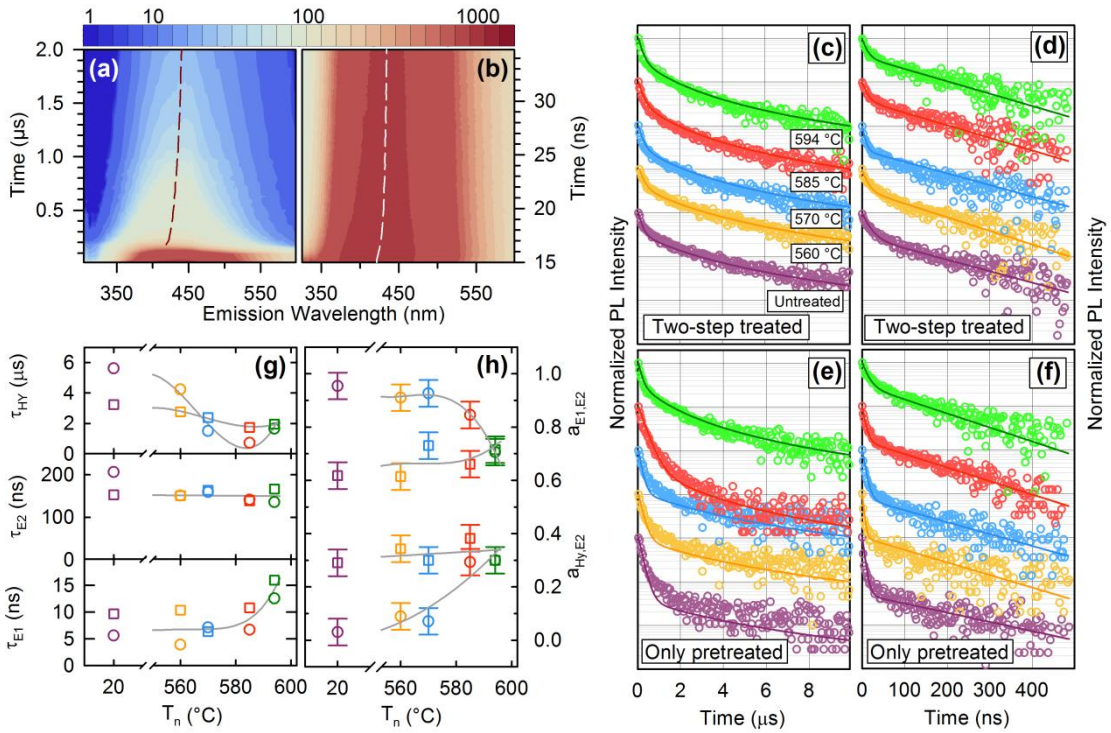

Figure 4. Representative time-resolved PL spectra excited at 250 nm in the (a) microsecond and (b) nanosecond domain of two-step treated $7.5Li_2O$-$2.5Na_2O$-$20Ga_2O_3$-$45GeO_2$-$25SiO_2$ sample pre-treated at 570 °C for 18 h. Dashed lines show PL band maximum shift *vs.* time. (c) Semi-log plot of PL decay curves (vertically shifted for clarity) in the μs domain (measured at 450 nm with excitation at 250 nm) and fitting curves, calculated according to Eq. 1, in nanocrystallized samples (after 30 min crystallization treatment at T_c) either without (curve 1) or after nucleation treatment at the indicated temperatures. (d) PL decay curves in the ns domain of the same samples in (c) and fitting curves with Eq. 2. (e) PL decay curves in the ns and (f) μs domain in samples not subjected to crystallization treatment (labels as in (c) and (d) as regards nucleation pre-treatment). (g) Time decay constants of hyperbolic component (τ_{Hy}) and fast and slow exponentials (τ_{E1} and τ_{E2}, respectively) from the fit of the decay curves in two-step treated (squares) and only-pretreated (circles) samples. (h) multiplicative factors in the fitting decay functions in Eqs. 1 and 2. Curves in (g) and (h) are guides for the eyes.

In Figs. 4c and 4d we report PL decay measurements in the μs and ns regimes, respectively, collected at 2.7 eV under pulsed excitation at 5 eV in material treated at T_c with and without nucleation pre-treatment at different T_n. The kinetics turns out to be hyperbolic in the μs regime (Fig. 4c) with decay lifetime τ_{Hy} of a few μs, except for the initial part following an exponential decay with τ_{E2} of 100-200 ns. The data are reproduced by a superposition of decays

$$f_{\mu s}(t) = a_{Hy,E2}\frac{1}{1+t/\tau_{Hy}} + (1-a_{Hy,E2})e^{-t/\tau_{E2}} \qquad (1)$$

where the hyperbolic decay arises from DAP recombination,[19,21] whereas the exponential part appears related to the UV component whose decay is responsible for the spectral shift just in the 10^{-1}-10^{0} μs region in Fig. 4a.

Such an exponential component is detected even better in the ns regime (Fig. 4d), accompanied by an additional exponential contribution with lifetime τ_{E1} shorter than 30 ns. This is related to the additional UV component responsible for the spectral shift in the 15-25 ns regime in Fig. 4b. Decay curves in the ns domain are reproduced by two exponentials

$$f_{ns}(t) = a_{E1,E2}e^{-t/\tau_{E1}} + (1-a_{E1,E2})e^{-t/\tau_{E2}}. \qquad (2)$$

Interestingly, exponentials and hyperbolic contributions are also found in only-pretreated material, both in μs (Fig. 4e) and ns (Fig. 4f) domain, with features similar to two-step treated samples. This points out – as also suggested by optical absorption and steady-state PL in Fig. 3a and 3b – that native phase-separated nuclei and nucleated nanophases at T_n (*i.e.* untreated and only-pretreated samples) are similar to γ-Ga_2O_3 as energy structure, optical gap, and decay paths.

However, despite all qualitative similarities, decay curves show some T_n-dependence and differences between only-pretreated and two-step treated samples, as registered by lifetimes τ_{E1}, τ_{E2}, and τ_{Hy} (Fig. 4g) and relative weights $a_{Hy,E2}$ and $a_{E1,E2}$ of the kinetic components (Fig. 4h). Some relevant facts give us some insights into the involved transitions.

Looking at the decay lifetime values (Fig. 4g), no relevant effect of T_n is detected on τ_{E2}, both before and after treatment at T_c, and only a moderate increase of τ_{E1} with T_n. By contrast, it is worth noting that the hyperbolic lifetime τ_{Hy} shows a clear T_n dependence, which in turn closely resembles the non-monotonic behaviour of nucleation-controlled NC size (Fig. 1d), except for the different range of values in only-pretreated and two-step treated samples. The hyperbolic decay lifetime is a probe of the two-

body (donor and acceptor) recombination kinetics, and can be used to obtain, to some extent, information on the number of acceptors per NC and the NC size. In fact, both parameters influence the mean distance between donor and acceptor and, in turn, the hyperbolic decay lifetime.[19] In Fig. 4g we register that τ_{Hy} decreases at increasing T_n, both before and after treatment, down to a minimum at the temperature of maximum nucleation rate (minimum NC size), suggesting a clear effect of size reduction on the mean donor-acceptor distance. Also, the wider τ_{Hy} range in only-pretreated material with respect to two-step treated samples points to an additional effect largely influencing the mean donor-acceptor distance in only-pretreated samples. Since τ_{Hy} of only-pretreated material is initially greater than in two-step treated, probably related to the number of acceptor per NC.

Looking at Fig. 4h, the factor $a_{Hy,E2}$ does not sensibly depend on T_n in two-step treated material, even though the emitted intensity greatly changes (Fig. 3c). Hyperbolic and slow exponential components, therefore, appear to behave as two decay channels of the same excitation event, regulated by a fixed branching ratio. The slow exponential decay may arise from recombination of excited donors in localized states, strictly competitive to DAP recombination within the single NC. Instead, in only-pretreated samples (circles in Fig. 4h), $a_{Hy,E2}$ increases with T_n, indicating that DAPs/donors ratio gradually increases in NC nuclei by increasing T_n. This suggests, quite reasonably, that donors (V_O sites) probably pre-exist to the more complex acceptor sites needed for DAPs and requiring nearby V_O and V_{Ga} sites.

As regards the relative weight of the fast components, we register larger $a_{E1,E2}$ in only-pretreated samples. Furthermore, $a_{E1,E2}$ decreases by increasing T_n (as a result of the weakening of the faster component with lifetime τ_{E1}) down to the value found in all samples treated at T_c, quite independently of T_n. Since the main NC features – size, number density, and interphase area – are different from sample to sample in two-step treated material, and are not decreasing functions of T_n in only-pretreated material, the fast exponential can hardly be related to the nanophase. It can instead be caused by light emitting sites in the glass matrix, whose fraction is constant in two-step treated samples (from XRD data), as the fast exponential component. Spectral position (at around 400 nm) and lifetime value (few ns) allow us to preliminary identify the kind of point defects potentially responsible for the fast violet component among the possible defect configurations compatible with a silica-based and germanosilicate glass matrix.[31] In Ge-containing silica-based glass, light emission in the violet spectral region is mainly expected from oxygen deficient defects consisting in two-fold coordinated O–Ge–O sites.[31-33] However, in such defects, the emission is ascribed to triplet-to-singlet transitions with decay time of 0.1 ms,[32] incompatible with the observed fast decay in the ns domain. Instead, violet luminescence with few ns of lifetime is typical of alkali-germanates and alkali-silicates,[34,35] arising from non-bridging groups 3O≡T–O–M with T=Si,Ge and M=Li,Na.[35]

Information from spectroscopic and kinetic analysis finally enable us to draw a picture of the relationships between nucleation process and resulting light emission features. In only-pretreated material, the monotonic PL enhancement vs T_n (Fig. 3c) indicates that the NC number change – which is not monotonic in the high-T_n range registered in the DSC analysis (Fig. 1b) – cannot fully explain the PL response. An additional key factor can be found in the formation of acceptors during nucleation, leading to the progressive reduction of DAP-free NCs that in the first steps of phase separation likely possess only donor sites. Increasing T_n, acceptor formation enables an increasing number of NCs to contribute to light emission via DAP recombination, which gradually overcomes less efficient decays from donor sites. This process is registered by the spectral band shift from UV to blue in only-pretreated samples (Fig. 3d), and by the enhancement of $a_{Hy,E2}$ ratio in Fig. 4h. In two-step treated samples, instead, $a_{Hy,E2}$ is almost constant and PL intensity reflects the change of NC number (determined by NC size at fixed nanophase amount), as shown by Fig. 3c and XRD and DSC data in Fig. 1. However, the maximum PL intensity is observed at T_n=570 °C, whereas τ_{Hy} reaches the smallest value at 585 °C, when mean NC size is minimized (squares in Fig. 4g). Possible source of PL decrease from 570 to 585 °C (Fig. 3c) is the occurrence of NC coalescence, as registered by bimodal size distribution in TEM analysis in Fig. 2e, with a resulting lowering of NC number. Additional factor of PL reduction at the highest T_n value, can also be acceptor passivation by removal of V_{Ga} by Li diffusion, since the higher T_n, the more likely the Li diffusion.

The occurrence of both effects, NC coalescence and Li diffusion, can be verified within the set of differently pretreated samples after intensifying the responsible processes by heating pretreated material at temperature significantly higher than T_c. In Fig. 5a we report XRD patterns of pretreated samples after heating from 20 °C to 980 °C (10 °C/min) followed by rapid cooling at room temperature. Besides additional reflections of gallium germanate and lithium gallium germanate secondary phases from matrix crystallization, the experiment registers three main modifications with respect to the patterns collected after treatment at T_c (Fig. 1): narrowing of all reflections of the main γ-Ga_2O_3 nanophase, weak reflections ascribable to $LiGa_5O_8$ and, importantly, modification of the intensity ratio between reflections at 36.3° and 64.2°, increasing by more than 12% by increasing the pretreatment temperature T_n from 585 to 594 °C. In Fig. 5b we report such results as T_n-dependence of NC size d_{NC}, estimated by Scherrer's relation from reflection width, and of the intensity ratio of the main nanophase reflections (whose value in γ-Ga_2O_3 and $LiGa_5O_8$ is 1.43 and 2.99, respectively, from PDF files).

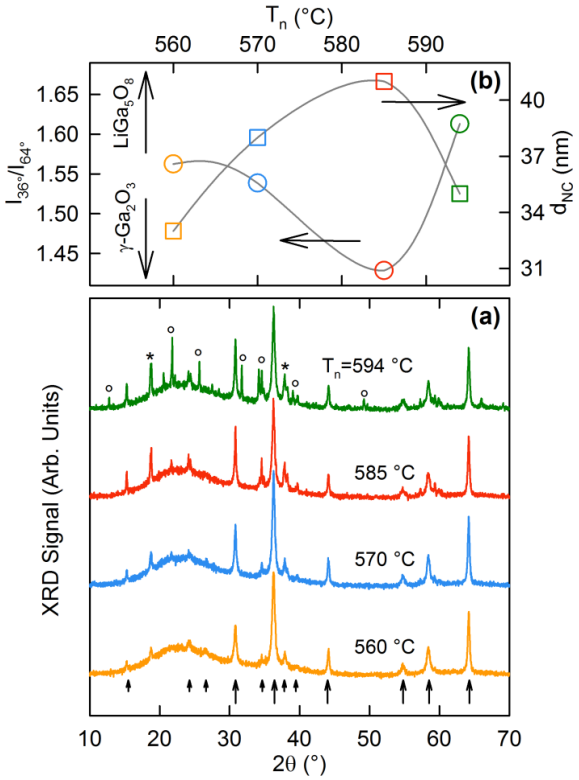

Figure 5. (a) XRD patterns of glass powders with composition $7.5Li_2O$-$2.5Na_2O$-$20Ga_2O_3$-$25SiO_2$-$45GeO_2$ pretreated at the indicated temperature for 18 h and then heated at 10 °C/min from room temperature up to 980 °C and rapidly quenched. Main reflections of γ-Ga_2O_3 and $LiGa_5O_8$ are indicated (long arrows and all arrows, respectively), together with main reflections of $LiGaGeO_4$ and $Ga_2Ge_2O_7$ secondary phases (circles and asterisks, respectively), according to PDF files 00-020-0426, 01-076-0199, 01-079-0213, and 00-035-0386, respectively. The patterns are vertically shifted for clarity. (b) Intensity ratio (circle, left axis) of the main reflections at 36.3° and 64.2° and Scherrer's NC size d_{NC} (square, right axis) determined by reflection broadening.

Therefore, on the one hand, the narrower reflections, with resulting d_{NC} values correlated with the T_n-dependence of the nucleation rate in Fig. 1b, confirms that the larger the NC number formed during nucleation pretreatment, the higher the probability of coalescence occurrence at higher temperature. Evidence of such an effect is found in the bimodal NC size distribution in Fig. 2, and can be the cause of the relatively lower PL intensity in two-step treated material after pretreatment at 585 °C compared with material pretreated at 570 °C, through a slightly lowering of NC density. On the other hand, the increase of the intensity ratio $I_{36°}/I_{64°}$ of the main γ-Ga_2O_3 reflections in material pretreated at 594 °C confirms that Li-diffusion into the nanophase is promoted by such pretreatment, and can be an additional cause of PL lowering through passivation of coordination defects and the related DAP population per NC.

Conclusions

Our analysis clarifies the composite nature of PL in wide-band-gap γ-Ga_2O_3 NCs in alkali-germanosilicate glass, showing that slow DAP recombination mechanism, responsible for light emission in the blue region, is coexistent with faster decays spectrally shifted in the UV. After analyzing DAP luminescence and the competitive light emission mechanisms as a function of NC nucleation rate by controlled pretreatment, the results suggest that nucleation can be used to tailor the light emission properties of the material. Specifically, we have found that luminescence is influenced not only by NC size change, and consequent modification of NC number density, but also by acceptor formation and V_{Ga} passivation. In such processes, the interaction between nanophase and glass matrix play a key role, providing the conditions for the occurrence of NC nucleation, NC coalescence, and Li incorporation, with a balance that depend on the nucleation temperature. As a result, new strategies can now be envisaged for the functionalization of wide-band-gap nanocrystals, tailoring light emission not only through size effects, but also through stoichiometry modifications promoted by controlled interaction with the host.

Acknowledgements

This work has been supported by the Ministry of Education and Science of the Russian Federation under Grant No. 11.G34.31.0027 and by Grant MK-1398.2014.3, and by Cariplo Foundation, Italy, under Project no. 2012-0920.

Notes and references

[a] P.D. Sarkisov International Laboratory of Glass-based Functional Materials, Mendeleev University of Chemical Technology of Russia, Miusskaya Square 9, 125190 Moscow, Russia.
[b] Istituto Italiano di Tecnologia, Via Morego 30, 16163 Genova, Italy.
[c] Department of Physics, University of Ferrara, via Saragat 1, 44100 Ferrara, Italy.
[d] Department of Materials Science, University of Milano-Bicocca, via Cozzi 55, 20125 Milano, Italy.
* Corresponding author's e-mail: alberto.paleari@unimib.it

1 A. I. Ekimov and A. A. Onushchenko, *JETP Lett.*, 1981, **34**, 345.
2. N. F. Borrelli, D. W. Hall, H. J. Holland and D. W. Smith, *J. Appl. Phys.*, 1987, **61**, 5399.
3. Y. Yin and A. P. Alivisatos, *Nature*, 2005, **437**, 664.
4. Yue Teng, Le Xin Song, A. Ponchel, Zheng Kun Yang, and Juan Xia, *Adv. Mater.*, 2014, **26**, 6238.
5. M. Kuno, *J. Phys. Chem. Lett.*, 2014, **5**, 3817.
6. J. Z. Zhang, J. K. Cooper and S. Gul, *J. Phys. Chem. Lett.*, 2014, **5**, 3694.
7. J. H. Yu, X. Liu, K. E. Kweon, J. Joo, J. Park, K.-T. Ko, D. W. Lee, S. Shen, K. Tivakornsasithorn, J. S. Son, J.-H. Park, Y.-W. Kim, G. S. Hwang, M. Dobrowolska, J. K. Furdyna and T. Hyeon, *Nature Mater.*, 2010, **9**, 47.
8. S. L. White, J. G. Smith, M. Behl and P. K. Jain, *Nature Commun.*, 2013, **4**, 2933.
9. N. Chiodini, F. Meinardi, F. Morazzoni, J. Padovani, A. Paleari, R. Scotti and G. Spinolo, *J. Mater. Chem.*, 2001, **11**, 926.
10. V. N. Sigaev, N. V. Golubev, E. S. Ignat'eva, B. Champagnon, D. Vouagner, E. Nardou, R. Lorenzi and A. Paleari, *Nanoscale*, 2013, **5**, 299.
11. S. Zhou, N. Jiang, B. Wu, J. Hao and J. Qiu, *Adv. Funct. Mater.*, 2009, **19**, 2081.
12. S. Chenu, E. Véron, C. Genevois, G. Matzen, T. Cardinal, A. Etienne, D. Massiot and M. Allix, *Adv. Optical Mater.*, 2014, **2**, 364.
13. S. Brovelli, A. Baraldi, R. Capelletti, N. Chiodini, A. Lauria, M. Mazzera, A. Monguzzi and A. Paleari, *Nanotech.*, 2006, **17**, 4031.
14. V. N. Sigaev, N. V. Golubev, E. S. Ignat'eva, V. I. Savinkov, M. Campione, R. Lorenzi, F. Meinardi and A. Paleari, *Nanotech.*, 2012, **23**, 015708.
15. A. C. Yanes, J. J. Velázquez, J. del-Castillo, J. Méndez-Ramos and V. D. Rodríguez, *Nanotech.*, 2008, **19**, 295707.
16. S. Chenu, E. Véron, C. Genevois, G. Matzen, T. Cardinal, A. Etienne, D. Massiot, and M. Allix, *Adv. Optical Mater.*, 2014, **2**, 364.
17. A. Paleari, S. Brovelli, R. Lorenzi, M. Giussani, A. Lauria, N. Mochenova and N. Chiodini, *Adv. Funct. Mater.*, 2010, **20**, 3510.
18. S. Brovelli, N. Chiodini, R. Lorenzi, A. Lauria, M. Romagnoli and A. Paleari, *Nature Commun.*, 2012, **3**, 690.
19. V. N. Sigaev, N. V. Golubev, E. S. Ignat'eva, A. Paleari and R. Lorenzi, *Nanoscale*, 2014, **6**, 1763.
20. S. Brovelli, N. Chiodini, F. Meinardi, A. Monguzzi, A. Lauria, R. Lorenzi, B. Vodopivec, M. C. Mozzati and A. Paleari, *Phys. Rev. B*, 2009, **79**, 153108.
21. M. Hedge, T. Wang, Z. L. Miskovic and P. V. Radovanovic, *Appl. Phys. Lett.*, 2012, **100**, 141903.
22. A. Paleari, V. N. Sigaev, N. V. Golubev, E. S. Ignat'eva, S. Bracco, A. Comotti, A. Azarbod and R. Lorenzi, *Acta Mater.*, 2014, **70**, 19.
23. V. M. Mashinsky, N. M. Karatun, V. A. Bogatyrev, V. N. Sigaev, N. V. Golubev, E. S. Ignat'eva, R. Lorenzi, M. C. Mozzati, A. Paleari, and E. M. Dianov, *Microsc. Microan.*, 2012, **18**, 259.
24. A. B. Seddon, V. K. Tikhomirov, H. Rowe and D. Furniss, *J. Mater. Sci.: Mater. Electron.*, 2007, **18**, S145.
25. R. R. Shaw and J. F. Breedis, *J. Am. Ceram. Soc.*, 1972, **55**, 422.
26. V. M. Fokin, A. A. Cabral, R. M. C. V. Reis, M. L. F. Nascimento and E. D. Zanotto, *J. Non-Cryst. Sol.*, 2010, **356**, 358.
27. A. Marotta, A. Buri and F. Branda, *J. Mater. Sci.*, 1981, **16**, 341.
28. K. E. Kelton, *J. Am. Ceram. Soc.*, 1992, **75**, 2449.
29. H. Y. Playford, A. C. Hannon, M. G. Tucker, D. M. Dawson, S. E. Ashbrook, R. J. Kastiban, J. Sloan, and R. I. Walton, *J. Phys. Chem. C*, 2014, **118**, 16188.
30. L. Binet and D. Gourier, *J. Phys. Chem. Solids* **1998**, *59*, 1241.
31. R. Salh, Silicon Nanocluster in Silicon Dioxide: Cathodo-luminescence, Energy Dispersive X-Ray Analysis, Infrared Spectroscopy Studies, Crystalline Silicon - Properties and Uses, 2011, Sukumar Basu (Ed.), ISBN: 978-953-307-587-7, InTech.
32. L. Skuja, *J. Non-Cryst. Solids*, 1998, **239**, 16.
33. B. Crivelli, M. Martini, F. Meinardi, A. Paleari, and G. Spinolo, *Phys. Rev. B*, 1996, **54**, 16637.
34. A. N. Trukin, J. Jansons, H.-J. Fitting, T. Barfels, and B. Schmidt, *J. Non-Cryst. Sol.*, 2003, **331**, 91.
35. A. N. Trukin, in Defects in SiO2 and related Dielectrics: Science and Technology, p.235, edited by G. Pacchioni, L. Skuja, D. Griscom, 2000 Kluwer Acad. Pub., The Netherlands.